Asymmetries in Coronal Spectral lines and Emission Measure Distribution

Durgesh Tripathi

Inter-University Centre for Astronomy and Astrophysics, Post Bag - 4, Ganeshkhind, Pune 411007, India

and

James A. Klimchuk

NASA Goddard Space Flight Center, Greenbelt, MD 20771, USA

ABSTRACT

It has previously been argued that 1. spicules do not provide enough pre-heated plasma to fill the corona, and 2. even if they did, additional heating would be required to keep the plasma hot as it expands upward. We here address the question of whether spicules play an important role by injecting plasma at cooler temperatures (< 2 MK), which then gets heated to coronal values at higher altitudes. We measure red-blue asymmetries in line profiles formed over a wide range of temperatures in the bright moss areas of two active regions. We derive emission measure distributions from the excess wing emission. We find that the asymmetries and emission measures are small and conclude that spicules do not inject an important (dominant) mass flux into the cores of active regions at temperatures > 0.6 MK ($\log T > 5.8$). These conclusions apply not only to spicules, but to any process that suddenly heats and accelerates chromospheric plasma (e.g., a chromospheric nanoflare). The traditional picture of coronal heating and chromospheric evaporation appears to remain the most likely explanation of the active region corona.

Subject headings: Sun: corona — Sun: atmosphere — Sun: transition region — Sun: UV radiation

1. Introduction

There has been great interest recently in fast ($\sim$ 100 km s^{-1}) upflows revealed by asymmetries in the profiles of hot spectral lines. These asymmetries take the form of small

enhancements in the blue wings of the lines. They have been measured by numerous authors using a variety of techniques, including double Gaussian fits and intensity differences between the red and blue sides of the profile (Hara et al. 2008; De Pontieu et al. 2009; McIntosh & De Pontieu 2009; Bryans et al. 2010; Martínez-Sykora et al. 2011; Tian et al. 2011, 2012; Doschek 2012; Brooks & Warren 2012). The asymmetries tend to be very subtle. They are best seen in faint areas at the peripheries of active regions, where the intensity of the secondary (upflow) component can exceed 20% of the intensity of the main ("rest") component. The intensity ratio is $< 5\%$ over most of the Sun.

It has been suggested that these upflows are associated with type II spicules (De Pontieu et al. 2009). Spicules originate in the chromosphere and are mostly cold, but limb observations from the Atmospheric Imaging Assembly (AIA; Lemen et al. 2012) on the Solar Dynamics Observatory (SDO) show that the tips of at least some type II spicules are heated to coronal temperatures as they are ejected (De Pontieu et al. 2011). The speeds of the proper motions seen at the limb are comparable to the Doppler shifts of the blue wing enhancements seen on the disk (~ 100 km s^{-1}). It was proposed that this hot spicule plasma may explain much or even most of the material that we observe in the corona. This would be a major shift from the conventional picture in which heating occurs in the corona itself, i.e., either the coronal plasma is maintained at high temperatures by quasi-steady heating, or else the plasma undergoes repeated cycles of impulsive heating (nanoflares) and evaporation, followed by slower cooling and draining.

Klimchuk (2012) recently examined the role of type II spicules in supplying the corona with hot plasma. He started with the hypothesis that all coronal plasma comes from spicules and examined the observational consequences. One test concerns the ratio of emission measure in the upflow to the emission measure in the downflow. Klimchuk (2012) found that, if the hypothesis of a spicule-dominated corona is correct, this ratio must exceed 3 in active regions, 1 in the quiet Sun, and 0.7 in coronal holes. He went on to argue that the temperatures of the upflow and downflow should be similar and therefore the emission measure ratio would approximately equal the ratio of blue wing to line core intensities in a typical coronal spectral line from species like Fe XIV. Since the observed ratios are much smaller than predicted, Klimchuk concluded that spicules can contribute at most a small fraction of the corona's hot plasma. In active regions, the discrepancy is two orders of magnitude. A second test involves the ratio of emission measures in the corona and lower transition region. Again the predicted and observed values disagree by two orders of magnitude. A third test was proposed involving the ratio of densities in the fast upflow and slow downflow. Patsourakos et al. (2013) recently found that the discrepancy is here, too, approximately two orders of magnitude. It appears that the quantity of hot plasma ejected into the corona by type II spicules—indeed by any mechanism that suddenly heats and accelerates chromo-

spheric plasma—is far less than the amount of hot plasma that exists in the corona.

Klimchuk (2012) also pointed out that, even if enough hot plasma were ejected, additional heating would be required at higher altitudes to compensate for the extreme adiabatic cooling that would otherwise occur as the plasma expands upward to fill the coronal flux tube. In the absence of heating, a 2 MK plasma at the tip of a spicule would cool to roughly 0.1 MK from expansion alone. Strong heating must therefore occur in the corona itself.

Even if spicules do not directly provide enough hot plasma to explain the corona, they might nonetheless eject large amounts of cooler plasma that is then heated to coronal temperatures at higher altitudes. We know that the bulk of a type II spicule is heated to < 0.1 MK as it is ejected (De Pontieu et al. 2011). However, this material falls back to the surface after reaching a maximum height of only 10^4 km, so it does not contribute to the coronal mass. Is it possible that a significant amount of material is heated to higher temperatures during the ejection, though still below 2 MK, and then later heated all the way to coronal values? This is the question that we address in this paper. Our approach is to determine the emission measure distribution of the ejected plasma by examining the excess blue wing emission of multiple spectral lines covering a range of temperatures. We note in passing that the spicule material that is only weakly heated to < 0.1 MK may explain the very bright emission from the lower transition region, which conventional coronal heating models cannot (Klimchuk 2012, although see Antiochos & Noci (1986) for an alternative explanation in mixed polarity quiet Sun regions).

Brooks & Warren (2012) have recently published results on emission measure distribution of excess blue wing emission observed in a faint "outflow" region at the periphery of an active region. As already mentioned, these are the places where line asymmetries are greatest. They are called outflow regions not because of the asymmetries, but because the line core is significantly Doppler shifted to the blue. It has been proposed that they may be an important source of slow solar wind (e.g., Sakao et al. 2007; Harra et al. 2008, see also Del Zanna et al. (2011) for an alternative explanation). Using double Gaussian fits, Brooks & Warren (2012) found that the EM of the secondary component peaks at 1.4–2.0 MK and decreases rapidly with temperature below 1 MK. The ratio of the EM at 0.6 MK ($\log T = 5.8$) to the maximum EM is generally < 0.01. In this faint outflow region, therefore, the EM determined from an Fe XIV line is a reasonable estimate of the total EM in the upflow.

Our study concerns bright moss areas within two active regions. Moss corresponds the footpoints of unresolved loops that form the generally hot and diffuse cores of active regions (e.g., Martens et al. 2000; Tripathi et al. 2008, 2010a). Any flows seen at these locations would be related to the mass balance of the core plasma. In particular, any spicules that supply mass to the core of active regions would occur here. As we will show, and has

been reported previously (e.g. Doschek 2012), line asymmetries are much smaller at these locations and are a significant challenge to measure. We therefore employ a new technique called Intensity Conserving Spline Interpolation (ICSI; Klimchuk et al. 2013). Even with this technique, we are only able to place upper limits on the EM of the excess wing emission. These upper limits are nonetheless extremely useful for evaluating the role of spicule upflows in supplying plasma to the corona.

2. Definition of RB-asymmetry

Following many other studies, we isolate the excess wing emission using the so-called red-blue (RB) asymmetry. Figure 1 displays a schematic Gaussian to demonstrate the RB asymmetry. We define the total emission in the blue wing of the spectral line within the velocity range v1 and v2 as:

$$I_B = \int_{-v1}^{-v2} I(v)\, dv = \sum I_i\ \Delta v = \Delta v \sum_i I_i, \tag{1}$$

where $\Delta\ v$ is the grid size. Similarly, the total emission in the red wing in the same velocity range towards the positive velocity side can be written as

$$I_R = \int_{v2}^{v1} I(v)\, dv = \sum I_i\ \Delta v = \Delta v \sum_i I_i. \tag{2}$$

If we consider that the emission in the core of the spectral line is part of a Gaussian profile given as

$$I(v) = I_0\ exp\left[-\left(\frac{v}{w}\right)^2\right], \tag{3}$$

where I_0 is the line center intensity, and w is the $1/e$ halfwidth, then the total emission in the Gaussian is

$$I_{core} = \sqrt{\pi}\ w\ I_0. \tag{4}$$

If the broadening is just because of thermal motions, then w can be written as

$$w = \frac{\lambda_0}{c} \sqrt{\frac{2kT}{M}}, \tag{5}$$

where λ_0 is the centroid of the line, T is the peak formation temperature, and M is the atomic mass of the ion. k is Boltzmann's constant and c is the speed of light.

The RB (Red-Blue) asymmetry can then be defined as

$$RB = \sqrt{\frac{1}{\pi}} \quad \frac{\Delta\ v}{w} \quad \frac{\sum I_B - \sum I_R}{I_0} \tag{6}$$

However, it is well known that in transition region and coronal spectral lines non-thermal broadening tends to dominate. In the present analysis, we have taken $w = 30$ km s^{-1} for all the spectral lines.

3. Observations

In this study we have analysed observations recorded by the Extreme-ultraviolet Imaging Spectrometer (EIS; Culhane et al. 2007) on board *Hinode*. We have used observations for two active regions, namely *AR 10961* and *AR 10953*. The EIS raster for the active region *AR 10961* was recorded on 2007 July 1 at 03:18 UT and is shown in Fig. 2. The left panel of the figure displays an image recorded in 171 Å from the Transition Region and Coronal Explorer (TRACE; Handy et al. 1999). The rectangular box on the TRACE image represents the field-of-view (FOV) of the EIS raster, which is 128″ by 128″. The 1″ slit with an exposure time of 25 s was used. An image obtained in Fe XII 195 Å from the raster is shown in the right panel of the figure. Also shown in the right panel are the two moss regions, namely 'A' and 'B' which are chosen for the analysis.

We have also studied the center-to-limb variation of the RB asymmetry and corresponding emission measure distribution. For this purpose we selected *AR 10953*. This active region was observed for five consecutive days (from May 01 to May 05, 2007) using the study sequence *CAM_ARTB_CDS_A*. During this time the active region moved from the disk center towards the western limb of the Sun. An image of the active region recorded by TRACE using the 171 Å passband on May 01, 2007 is shown in Fig. 3. The box on the TRACE image shows the EIS field of view. A corresponding image obtained in Fe XII 195 Å is shown in the right panel. This study sequence takes about 20 minutes to raster a FOV of 200″ by 200″ with an exposure time of 10 s using the 2″ slit. The moss region which was tracked is shown in Fig. 4 by an arrow.

The rasters used here have been studied earlier for different purposes and the details can be found in Tripathi et al. (2008, 2010a) for *AR 10953* and in Tripathi et al. (2010b, 2011) for *AR 10961*. We have applied standard data processing software provided in *solarsoft* (Freeland & Handy 1998) to each dataset.

4. Data Analysis and Results

In order to derive the RB asymmetry, it is important to compute the line center position (LCP) as accurately as possible. A variety of methods have been used. De Pontieu et al. (2009) fitted a single Gaussian to the full line profile. Martínez-Sykora et al. (2011) noted that such a fit will be influenced by any excess wing emission, which will in turn bias the computed RB asymmetry, so they fitted a single Gaussian to the line core only. Tian et al. (2011) fitted a double Gaussian to the full profile and set the LCP equal to the position of the main component. In all cases, the data are mapped onto a finer spectral grid (typically 10 times finer) so that the summations in equations (1) and (2) can be computed. Presumably a spline interpolation is used, though details are not generally provided in the papers. In yet another method, the LCP is taken to be the position of peak intensity in the interpolated (higher resolution) profile (Tian et al. 2011)

To explore how sensitively the computed RB asymmetry depends on the LCP, we first compare several different options (see also Tian et al. (2011)). We use the central positions of single Gaussian fits and the positions of peak intensity in spline interpolations. Cognizant of the concerns raised by Martínez-Sykora et al. (2011), we consider both the full line profile and subsets of the profile in the line core. The different options are:

1. Single Gaussian fit to the complete spectral line profile [case 1]
2. Single Gaussian/spline fit to two blue points and one red point [case 2]
3. Single Gaussian/spline fit to two blue and two red points [case 3]
4. Single Gaussian/spline fit to one blue point and two red points [case 4]

where the blue and red points in the profile are defined with respect to the data point with maximum intensity across the original (low resolution) profile.

To determine the RB asymmetry, the steps we follow are as follows:

1. We determine the reference wavelength by performing either a spline or a Gaussian fit using 4 or 5 points in the core of the line profile or the complete line profile depending

Table 1: Peak intensity, line centre (reference wavelength) and the RB symmetry obtained in different scenarios using Gaussian fitting and spline fitting.

Fitting		Peak Intensity [erg cm^{-2} s^{-1} sr^{-1}]	LCP [Å]	RB Asymmetry
Gaussian	Case 1	30126.1	202.05001	0.00
	Case 2	29850.1	202.04917	−0.02
	Case 3	30124.4	202.04956	−0.01
	Case 4	30124.5	202.04956	−0.01
Spline	Case 2	30124.5	202.04687	−0.08
	Case 3	30126.4	202.04787	−0.06
	Case 4	30126.3	202.04795	−0.05
ICSI		31073.3	202.04746	− 0.06

on the scenario under consideration. The reference wavelength is where the fit has peak intensity.

2. We map the original data onto a 25 times finer grid using a spline fit on all the points in the profile, including the wings and convert from a wavelength scale to velocity scale assigning zero velocity to the LCP.

3. Then compute the RB asymmetry from ±50 to ±120 km s^{-1} using the method described in section 2.

For our purposes here, we restrict our attention to the Fe XIII λ202 line, which is considered to be one of the cleanest spectral lines present in the EIS spectra. Throughout our study, we use spectra that are spatially averaged over the selected moss regions in order to improve the signal-to-noise. For this comparison of LCP methods, we only use moss region A shown in Figure 2.

Table 1 shows the peak intensity, line centroid and RB asymmetry obtained by considering different scenarios for Gaussian and spline fitting. The LCP has moved toward the red side from case 2 to case 4 for Gaussian fitting and from case 1 to case 3 for spline fitting case. The RB asymmetry obtained for case 1 using Gaussian fitting is negligible. Note that the negative (positive) values of RB asymmetry suggest red (blue) wing enhancement. For Gaussian fitting cases 2, 3 & 4 the intensity in the red wing is larger then in blue wing. However, the difference in obtained asymmetry is only about 1%. For spline fitting, in all

three cases, there is an enhancement in the red wing that decreases from about 8% for case 2 to 5% for case 4.

These results suggest that the small RB asymmetries depend very sensitively on the LCP. We performed a simple analytical calculation to understand this better. We took the same observed profile and computed the RB asymmetry for many different values of the LCP ranging between ±0.25 from the position obtained using the case 3 Gaussian fit. The results show that an LCP difference of only 0.00067 Å (one-thirtieth of an EIS spectral bin, or approximately 1 km s^{-1} at 200 Å) produces an RB difference of 0.018. This suggests that the previously published measurements of RB asymmetries have considerable uncertainty and should be treated with great caution whenever the asymmetry is only a few percent.

We know that the intensity we observe in a spectral bin is the mean intensity averaged over the bin. It is traditionally assigned to the wavelength at the center of the bin. However, this is only appropriate if the line profile is linear within the bin. This is generally not the case. If the line profile is curved, then the mean intensity should really be assigned to a position that is offset from the bin center. Alternatively, the intensity assigned to the center should be different from the mean intensity. Klimchuk et al. (2013) have recently developed a new method called Intensity Conserving Spline Interpolation (ICSI) that takes this into account. It is an iterative method that, as the name implies, conserves intensity in every spectral bin. Traditional spline fitting routines do not conserve intensity when they force the fit to have an intensity equal to the mean at a position midway in the bin. This can lead to significant errors, especially in determining the LCP of the profile. All RB asymmetry results presented throughout the remainder of the paper use the ICSI method to map the original data onto a 100 times finer spectral grid. The LCP is taken to be the position of peak intensity in the high resolution profile. The last row in Table 1 provides the peak intensity, LCP and RB asymmetry obtained using the ICSI method.

4.1. Asymmetries in different spectral lines for two moss regions A and B

We first considered moss regions A & B in active region *AR10961* shown in Figure 2. We measured the RB asymmetry of Si VII 275.36 Å, Fe X 184.53 Å, Fe XII 192.42 Å, Fe XIII 202.04 Å, Fe XIV 264.79 Å, Fe XV 284.16 Å and Fe XVI 263.98 Å. Figure 5 shows the Fe spectral lines from moss region A over-plotted with the ICSI fits. Notice that the intensity integrated under the curve in each bin is equal to the intensity of the original histogram. This is especially important near the peak of the profile, where the LCP is determined.

The difference of intensities between blue and red wings and corresponding RB asym-

metry (RBA) are tabulated in Table 2. Except for Si VII and Fe XV, the intensity differences and corresponding RBAs are negative, indicating excess red wing emission. The magnitudes of the RBAs are generally well below 5% and in no case exceed 10%. They are largest at intermediate temperature (Fe X, XII, and XIII).

We used the Pottasch method (Pottasch 1963; Tripathi et al. 2010a) to derive emission measures from the intensity differences. Figure 6 displays the EM(T) distributions for moss regions A and B, where we have given the EM the same sign as the asymmetry. The results are similar for regions A and B. The EM has a very small value at $\log T = 5.8$, becomes progressively larger (more negative) as temperature increases, then suddenly becomes smaller at $\log T = 6.3$. The trend of increasing magnitude with temperature is reminiscent of what Brooks & Warren (2012) found, except they detected excess blue emission rather than excess red emission. Also, they observed a faint outflow region rather than moss.

Table 2: Reference wavelength and RB asymmetry obtained for different spectral line for moss regions A and B using ICSI.

Ion	Region A		Region B	
	I_B - I_R [erg cm^{-2} s^{-1} sr^{-1}]	RBA	I_B - I_R [erg cm^{-2} s^{-1} sr^{-1}]	RBA
Si VII	3.14	0.027	1.43	0.011
Fe X	–29.61	–0.056	–27.49	–0.095
Fe XII	–20.52	–0.032	–32.11	–0.049
Fe XIII	–69.66	–0.063	–50.00	–0.042
Fe XIV	–20.47	–0.014	–5.65	–0.005
Fe XV	69.93	0.009	80.99	0.016
Fe XVI	–4.32	–0.009	–4.52	–0.017

4.2. Center to limb variation of asymmetries in different spectral lines

We next studied the center-to-limb variation of the RBA for the moss region in active region *AR10953* shown in Figure 3. Center-to-limb variations are important for understanding time evolution and geometry (line of sight) effects. For example, the center-to-limb behavior of the RBA in the faint outflow regions studied by Bryans et al. (2010) and Tian et al. (2012) indicate high-speed upflows inclined outward from the center of the active region. This is the expected tilt of the magnetic field at the periphery of the active region where the outflow

regions are located. As pointed out by Tian et al. (2012), this is also strong evidence that the RBAs are not artifacts of blends. Blends would have an equivalent effect at all disk locations, not preferentially at disk center or the east limb or the west limb.

Table 3 shows the intensity differences and RBAs tracked over 5 days. The EM(T) distributions are plotted in Figure 7. A combination of positive (enhanced blue wing) and negative (enhanced red wind) values are present. The magnitudes of the asymmetries are small. The largest is 4.5%, and most are $< 2\%$. The measurements have a rather random appearance, with no obvious patterns, either in temperature or in time. The only consistency is that the EM is very small at $\log T = 5.8$ on all of the days.

5. Summary and Discussion

The measurements presented in Tables 2 and 3 and Figures 6 and 7 paint a confusing picture. The situation is made worse if we combine EM distributions from the two figures in a single plot. We are forced to conclude that the RBA and EM measurements are likely dominated by uncertainties. This should not be surprising, given the discussion in Section 4 and the fact that the measured RBA values are very small. A 2% RBA is equivalent to an error in the line center position (LCP) of less than one-thirtieth of an EIS spectral bin.

The measurements are nonetheless extremely useful for placing upper limits on the emission measure of any rapidly flowing material that would emit in the line wings. The most consistent aspect of our measurements is the EM at $\log T = 5.8$. At all moss locations and on all days, EM $< 4 \times 10^{25}$ cm^{-5} at this lowest temperature. At the other temperatures, EM is mostly $< 5 \times 10^{26}$ cm^{-5}. However, since the sign of the asymmetry varies in seemingly random ways, we suggest that the true EM is actually smaller and masked by errors in the measurements.

Table 3: Centre to limb variation of asymmetry for different spectral lines.

Ion	May 01		May 02		May 03		May 04		May 05	
	I_B - I_R	RBA	I_B - I_R	RBA	I_B - I_R	RBA	I_B - I_R	RBA	I_B - I_R	RBA
Si VII	2.52	0.021	2.37	0.022	0.10	0.001	1.00	0.008	1.00	0.007
Fe XII	-10.65	–0.020	4.46	0.008	13.89	0.022	-20.60	-0.031	29.69	0.045
Fe XIII	-33.56	-0.042	-22.08	-0.027	12.38	0.012	-2.86	-0.002	-1.88	-0.001
Fe XIV	4.14	0.003	7.01	0.005	68.01	0.036	-47.52	-0.024	27.26	0.018
Fe XV	-76.53	-0.012	186.11	0.034	-91.86	-0.009	278.79	0.033	140.63	0.019
Fe XVI	3.58	0.008	5.70	0.012	16.30	0.022	-15.77	-0.021	1.67	0.004

We can compare these upper limits with the EM we measured previously in the inter-moss regions. For *AR10961* the inter-moss EM peaks at about 10^{28} cm^{-5}, and for *AR10953* it peaks at about 3×10^{28} cm^{-5} (Tripathi et al. 2011). These inter-moss measurements represent the coronal plasma that is magnetically linked to the plasma at the moss footpoints. We can therefore compare the emission measures in the same way that Klimchuk (2012) did for blue wing and line core emission of individual hot coronal lines. We find that the EM of the rapidly upflowing plasma is approximately two orders of magnitude less than the EM of the stationary (or slowly downflowing) plasma contained within the same magnetic loops. In stark contrast, Klimchuk argued that the EM of the upflow would need to exceed the EM of the downflow if type II spicules are the primary source of coronal plasma.

In summary, Klimchuk (2012) showed that 1. spicules do not provide enough pre-heated plasma to fill the corona, and 2. even if they did, additional heating would be required to keep the plasma hot as it expands upward. The question remained as to whether spicules can help explain the corona by injecting plasma at cooler temperatures (< 2 MK), which then gets heated to coronal values at higher altitudes. Our study indicates that this is not the case in active regions, at least for injection temperatures > 0.6 MK ($\log T > 5.8$). Spicules carry a large mass flux at much cooler temperatures (< 0.1 MK), but most of this mass falls back to the surface in cool state after reaching a maximum height of about 10^4 km. We are aware of no evidence for a large upward mass flux at in the range $0.1 < T < 0.6$ MK, but further investigation is warranted.

We end by noting that these conclusions apply not only to spicules, but to any process that suddenly heats and accelerates chromospheric plasma (e.g., a chromospheric nanoflare). We conclude that the traditional picture of coronal heating and chromospheric evaporation remains the most likely explanation of the corona.

Hinode is a Japanese mission developed and launched by ISAS/JAXA, collaborating with NAOJ as a domestic partner, NASA and STFC (UK) as international partners. Scientific operation of the Hinode mission is conducted by the Hinode science team organized at ISAS/JAXA. This team mainly consists of scientists from institutes in the partner countries. Support for the post-launch operation is provided by JAXA and NAOJ (Japan), STFC (U.K.), NASA, ESA, and NSC (Norway). CHIANTI is a collaborative project involving researchers at NRL (USA) RAL (UK), and the Universities of Cambridge (UK), George Mason (USA), and Florence (Italy). The work of JAK was supported by the NASA Supporting Research and Technology Program. The authors benefited from participation in the International Space Science Institute team led by S. Bradshaw and H. Mason. The authors also thank H. Mason and P. R. Young for various discussions.

REFERENCES

Antiochos, S. K., & Noci, G. 1986, ApJ, 301, 440

Brooks, D. H., & Warren, H. P. 2012, ApJ, 760, L5

Bryans, P., Young, P. R., & Doschek, G. A. 2010, ApJ, 715, 1012

Culhane, J. L., et al. 2007, Sol. Phys., 243, 19

De Pontieu, B., McIntosh, S. W., Hansteen, V. H., & Schrijver, C. J. 2009, ApJ, 701, L1

De Pontieu, B., et al. 2011, Science, 331, 55

Del Zanna, G., Aulanier, G., Klein, K.-L., & Török, T. 2011, A&A, 526, A137

Doschek, G. A. 2012, ApJ, 754, 153

Freeland, S. L., & Handy, B. N. 1998, Sol. Phys., 182, 497

Handy, B. N., et al. 1999, Sol. Phys., 187, 229

Hara, H., Watanabe, T., Harra, L. K., Culhane, J. L., Young, P. R., Mariska, J. T., & Doschek, G. A. 2008, ApJ, 678, L67

Harra, L. K., Sakao, T., Mandrini, C. H., Hara, H., Imada, S., Young, P. R., van Driel-Gesztelyi, L., & Baker, D. 2008, ApJ, 676, L147

Klimchuk, J. A. 2012, Journal of Geophysical Research (Space Physics), 117, 12102

Klimchuk, J. A., Patsourakos, S., & Tripathi, D. 2013, ApJ, in preparation

Lemen, J. R., et al. 2012, Sol. Phys., 275, 17

Martens, P. C. H., Kankelborg, C. C., & Berger, T. E. 2000, ApJ, 537, 471

Martínez-Sykora, J., De Pontieu, B., Hansteen, V., & McIntosh, S. W. 2011, ApJ, 732, 84

McIntosh, S. W., & De Pontieu, B. 2009, ApJ, 707, 524

Patsourakos, S., Klimchuk, J. A., & Young, P. R. 2013, ApJ, Submitted

Pottasch, S. R. 1963, ApJ, 137, 945

Sakao, T., et al. 2007, Science, 318, 1585

Tian, H., McIntosh, S. W., De Pontieu, B., Martínez-Sykora, J., Sechler, M., & Wang, X. 2011, ApJ, 738, 18

Tian, H., McIntosh, S. W., Xia, L., He, J., & Wang, X. 2012, ApJ, 748, 106

Tripathi, D., Klimchuk, J. A., & Mason, H. E. 2011, ApJ, 740, 111

Tripathi, D., Mason, H. E., Del Zanna, G., & Young, P. R. 2010a, A&A, 518, A42

Tripathi, D., Mason, H. E., & Klimchuk, J. A. 2010b, ApJ, 723, 713

Tripathi, D., Mason, H. E., Young, P. R., & Del Zanna, G. 2008, A&A, 481, L53

This preprint was prepared with the AAS LaTeX macros v5.2.

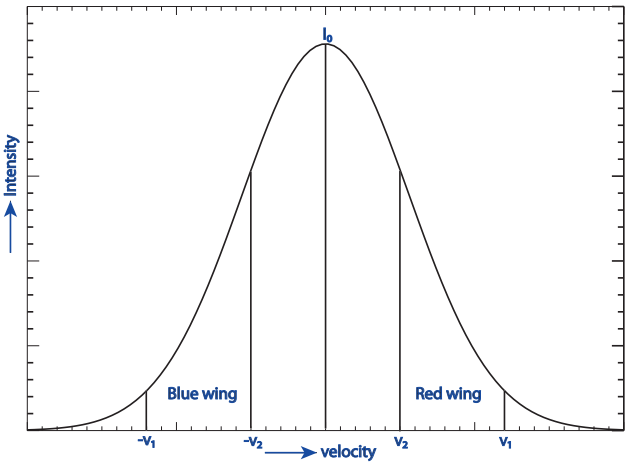

Fig. 1.— A schematic of a line profile to demonstrate the definition of RB asymmetry

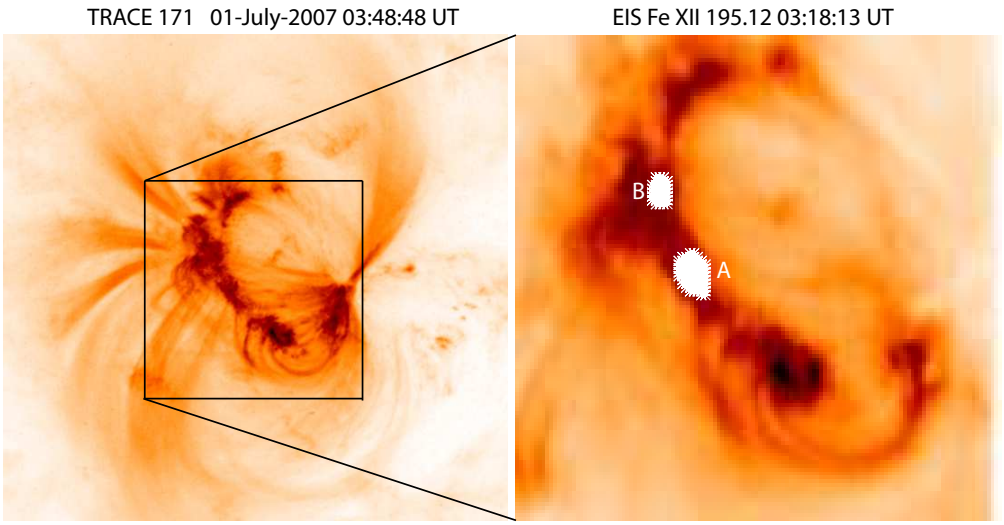

Fig. 2.— Left panel: AR 10961 observed by TRACE on July 01, 2007. The rectangular box show the EIS FOV. Right panel: EIS image obtained in Fe XII line. Regions A and B are the identified moss regions for the study of RB asymmetry. The figure is adopted from Tripathi et al. (2010b)

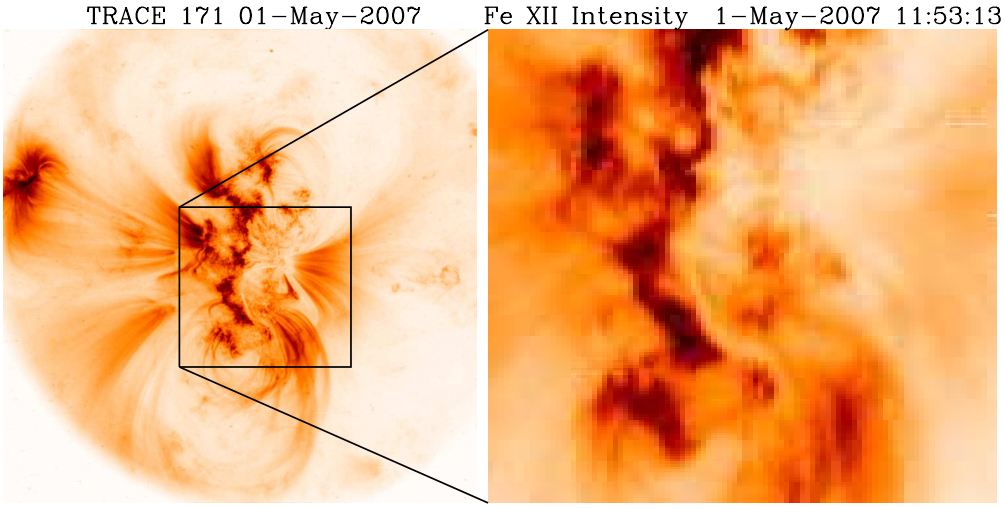

Fig. 3.— Left panel: AR 10953 observed by TRACE on May 01, 2007. The rectangular box show the EIS FOV. Right panel: EIS image obtained in Fe XII line.

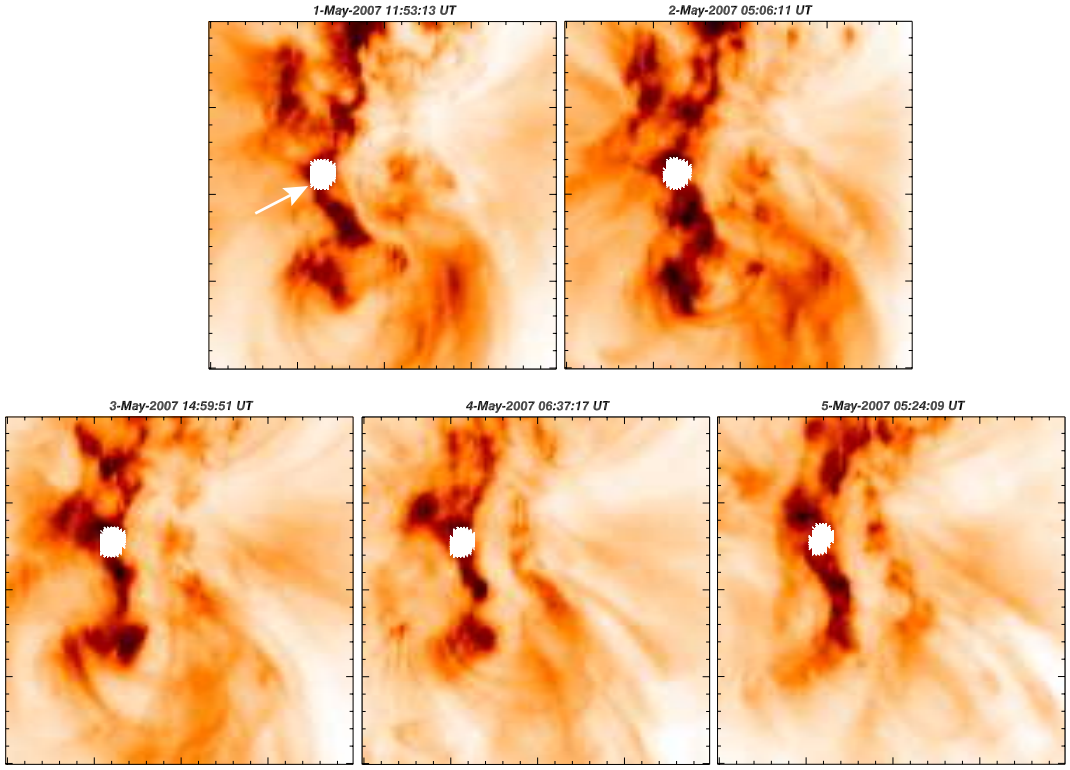

Fig. 4.— EIS Fe XII images of AR 10953 observed for five consecutive days. The marked regions is identified moss region for which the RB asymmetry is studied.

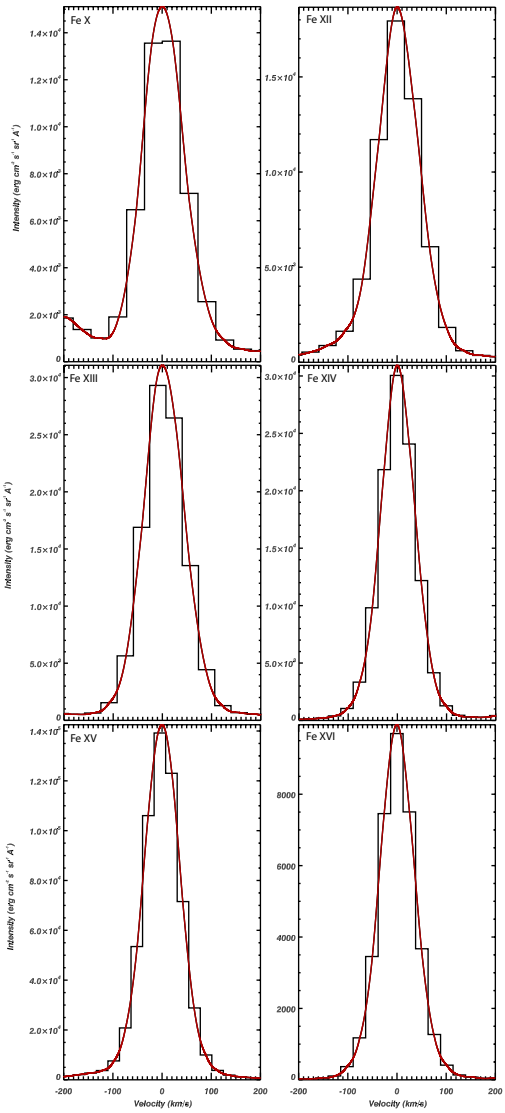

Fig. 5.— Spectral profile from Fe X to Fe XVI. The fit is obtained by the method proposed by Klimchuk et al. (2013).

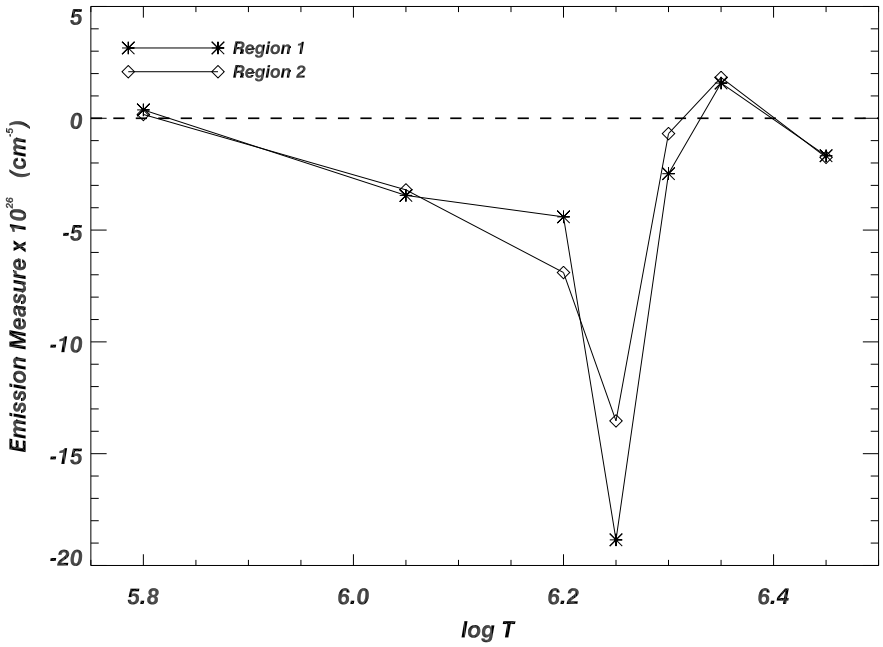

Fig. 6.— Emission measure distribution obtained using the difference in intensities in moss A and B.

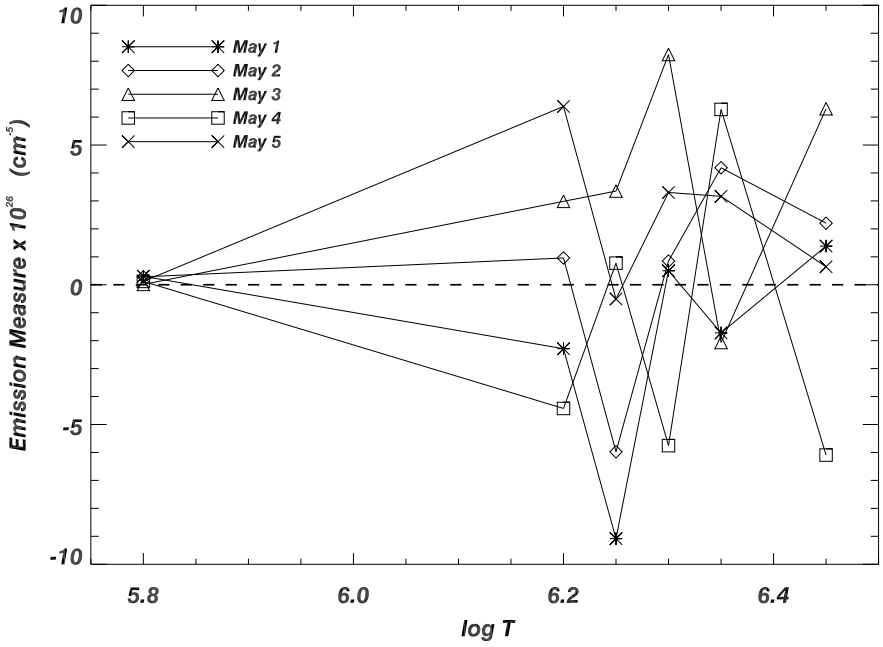

Fig. 7.— Emission measure distribution obtained using the difference in intensities in moss region tracked for five consecutive days.